Optical storage of high-density information beyond the diffraction limit: A quantum study

V. Delaubert,[1] N. Treps,[1] G. Bo,[2] and C. Fabre[1]
[1]*Laboratoire Kastler Brossel, UPMC, Case 74, 4 Place Jussieu, 75252 Paris Cedex 05, France*
[2]*Laboratoire Pierre Aigrain, Ecole Normale Supérieure, 24 rue Lhomond, 75231 Paris Cedex 05, France*
(Received 13 September 2005; revised manuscript received 28 November 2005; published 27 January 2006)

We propose an optical readout scheme allowing a proof of principle of information extraction below the diffraction limit. This technique, which could lead to improvement in data readout density onto optical disks, is independent from the wavelength and numerical aperture of the reading apparatus, and involves a multipixel array detector. Furthermore, we show how to use nonclassical light in order to perform a bit discrimination beyond the quantum noise limit.

DOI: 10.1103/PhysRevA.73.013820 PACS number(s): 42.50.Dv, 42.30.Va, 42.30.Wb

I. INTRODUCTION

The reconstruction of an object from its image beyond the diffraction limit, typically of the order of the wavelength, is a hot field of research, though a very old one, as Bethe already dealt with the theory of diffraction by subwavelength holes in 1944, to the best of our knowledge [1]. More recently, a theory has been developed to be applied to the optical storage problem, in order to study the influence of very small variations of pit width or depth relative to the wavelength [1–6]. To date, only a few super-resolution techniques [7] include a quantum treatment of the noise in the measurement, but to our knowledge, none has been applied to the optical data storage problem.

Optical disks are now reaching their third generation, and have improved their data capacity from 0.65 Gbytes for compact disks (using a wavelength of 780 nm), to 4.7 Gbytes for DVDs ($\lambda=650$ nm), and eventually to 25 GB for the Blu-Ray disks (using a wavelength of 405 nm). In addition to new coding techniques, this has been achieved by reducing the spot size of the diffraction-limited focused laser beam onto the disk, involving higher numerical apertures and shorter wavelengths.

Several further developments are now in progress, such as the use of volume holography, 266 nm reading lasers, immersion lenses, near field systems, multidepths pits [8], or information encoding on angle positions of asymmetrical pits [9]. These new techniques rely on a bit discrimination using small variations of the measured signals. Therefore, the noise is an important issue, and ultimately, quantum noise will be the limiting factor.

In this paper, we investigate an alternative and complementary way to increase the capacity of optical storage, involving the retrieval of information encoded on a scale smaller than the wavelength of the optical reading device. We investigate a way to optimize the detection of subwavelength structures using multipixel array. With an attempt to a full treatment of the optical disk problem being far too complex, we have chosen to illustrate our proposal on a very simple example, leaving aside most technical constraints and complications, but still involving all the essence of the overall problem.

We first explain how the use of an array detector can lead to an improvement of the detection and distinction of subwavelength structures present in the focal spot of a laser beam. We then focus on information extraction from an optical disk with a simple but illustrative example, considering that only a few bits are burnt on the dimensions of the focal spot of the reading laser, and show how the information is encoded from the disk to the light beam, propagated to the detector, and finally detected. We explain the gain configuration of the array detector that has to be chosen in order to improve the signal-to-noise ratio of the detection. Moreover, as quantum noise is experimentally accessible, and will be a limiting factor for further improvements, we perform a quantum calculation of the noise in the detection process. Indeed, we present how this detection can be optimized to perform simultaneous measurements below the quantum noise limit, using nonclassical light.

II. PROPOSED SCHEME FOR BIT SEQUENCE RECOGNITION IN OPTICAL DISKS

We propose an optical readout scheme shown in Fig. 1 allowing information extraction from optical disks beyond the diffraction limit, based on the multipixel detection. Bits, coded as pits and holes on the optical disk, induce phase flips in the electric field transverse profile of the incident beam at reflection. The reflected beam is imaged in the far field of the disk plane, where the detector stands. In the far field, the phase profile induced by the disk is converted into an intensity profile, that the multipixel detectors can, at least partly, reconstruct.

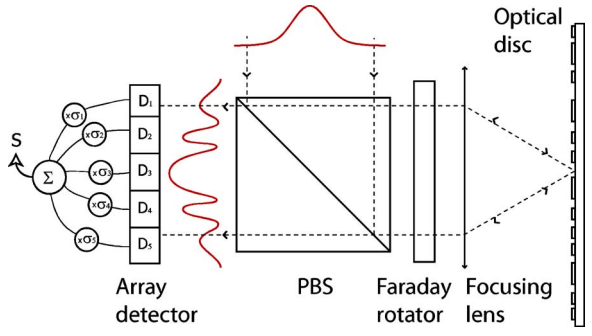

FIG. 1. (Color online) Scheme for information extraction from optical disks, using an array detector.

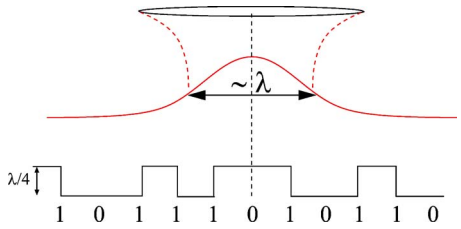

FIG. 2. (Color online) Example of a bit sequence on an optical disk. The spacing between the bits is smaller than the wavelength, the minimum waist of the incident laser beam being of the order of λ. A hole depth of λ/4 insures a π phase shift between fields reflected on a pit and a hole.

Taking into account that a lot of *a priori* information is available—i.e., only a finite number of intensity profiles is possible—we propose to use a detector with a limited number of pixels D_k whose gains can independently be varied depending on which bit sequence one wants to detect. The signal is then given by

$$S = \sum_k \sigma_k N_k, \tag{1}$$

where N_k is the mean photon number detected on pixel D_k, and σ_k is the electronic gain of the same pixel. Ideally, to each bit sequence present on the disk corresponds a set of gains chosen so that the value of the measurement is zero, thus canceling noise from the mean field. Measuring the signal for a given time interval T around the centered position of a bit sequence in the focal spot, and testing, in parallel, all the predefine sets of gain in the remaining time, allows us to deduce which bit sequence is present on the disk.

We will first show that this improvement in a density of information encoded on an optical disk is already possible using classical resources. Moreover, as the measurement is made around a zero mean value, the classical noise is mostly canceled. Hence, we reach regimes where the quantum noise can be the limiting factor. We will demonstrate how to perform measurements beyond the quantum noise limit, using previous results on quantum noise analysis in multipixel detection developed in Ref. [10].

III. ENCODING INFORMATION FROM A DISK ONTO A LIGHT BEAM

We have explained the general principle of readingout subwavelength bit sequences encoded on an optical disk, and now focus on the information transfer from the optical disk to the laser beam, through an illustrative example.

Let us recall that bits are encoded by pits and holes on the disk surface: a step change from hole to pit (or either from pit to hole) encodes bit 1, whereas no depth change on the surface encodes bit 0, as represented in Fig. 2. A hole depth of λ/4 ensures a π phase shift between the fields reflected by a pit and a hole. In this section, we compute the incident field distribution on the optical disk affected by the presence of a bit sequence in the focal spot, and finally analyze the intensity back reflected in the far field, in the detection plane, as sketched in Fig. 1.

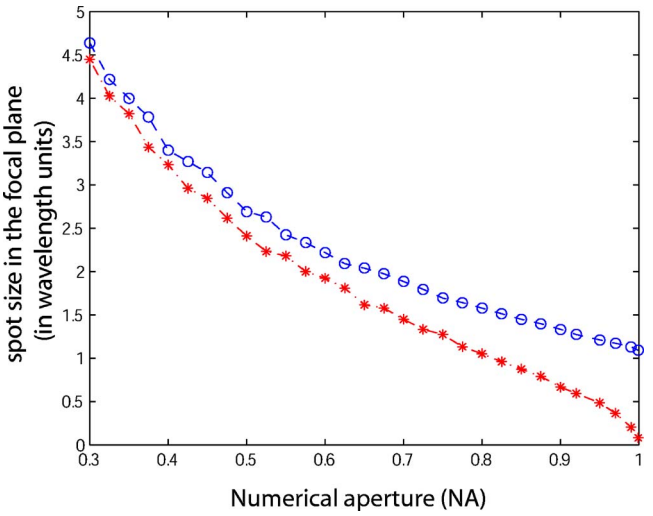

FIG. 3. (Color online) Evolution of the focused spot size of an incident plane wave with the numerical aperture (for λ=780 nm in air medium). The spot size is limited to the order of the wavelength in the nonparaxial case (○), whereas it goes to zero for very high numerical apertures in the paraxial case (∗).

A. Beam focalization

Current optical disk readout devices involve a linearly polarized beam strongly focused on the disk surface to point out details whose size is of the order of the laser wavelength. The numerical aperture (NA) of the focusing lens can be large (0.47 for CDs, 0.6 for DVDs, and 0.85 for BLU RAY disks), and the exact calculation of the field cannot be done in the paraxial and scalar approximation. Thus, the vectorial theory of diffraction has to be taken into account.

The structure of the electromagnetic field in the focal plane of a strongly focused beam has been investigated for decades now [11], as its applications include areas such as microscopy, laser microfabrication, micromanipulation, and optical storage [12–19].

In our case of interest, we can restrict the field calculation to the focal plane, which is the disk plane. Thus Richards and Wolf integrals [20], that are not suitable for a general propagation of the field, but which can provide the field profile in the focal plane for any type of polarization of the incoming beam as long as the focusing length is much larger than the wavelength, can be used to achieve this calculation. These integrals have already been used in many publications dealing with tight focusing processes [21–28]. As highlighted in these references, the importance of the vectorial aspect of the field can easily be understood when a linearly polarized beam is strongly focused, as the polarization of the wave after the lens is not perpendicular to the propagation axis anymore and has thus components along this axis. In order to estimate the limit of validity of the paraxial approximation, we computed focused spot sizes of linearly polarized beams in the focal plane for different numerical apertures, first in the paraxial approximation, and then calculated with Richards and Wolf integrals. The results are compared in Fig. 3 for an incident plane wave in an air medium with λ=780 nm, where the spot size is defined as the diameter

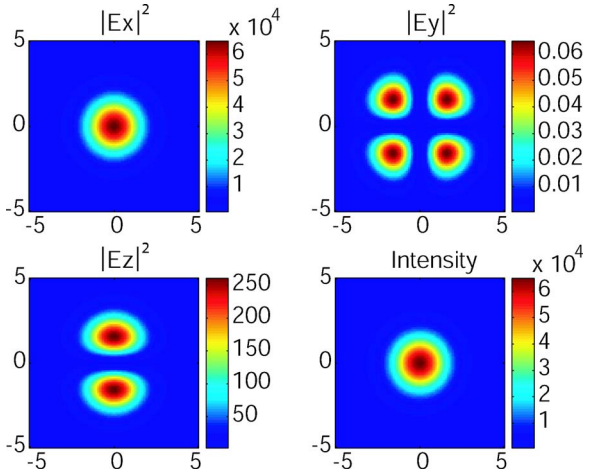

FIG. 4. (Color online) Norm of the different field components and resultant intensity in the focal plane with a linearly polarized incident field along the x axis, focused with a 0.47 numerical aperture.

which contains 86% of the focused energy, as in Ref. [29]. We see that when the numerical aperture exceeds 0.6, a good prediction requires a nonparaxial treatment. Moreover, whereas there is no theoretical limit to focalization in the paraxial case, we see that nonparaxial effects prevent us to reach a waist smaller than the order of the wavelength. Note that this limit is not fundamental and can be overcome by modifying the polarization of the incoming beam. Quabis and co-workers have indeed managed to reduce the spot area to about 0.1 λ^2 using an incident radially polarized doughnut beam [21,24].

As our aim is to present a demonstration of principle and not a full treatment of the optical disk problem, the following calculations will be done using the physical parameters of the actual compact disks (λ=780 nm and NA=0.47, corresponding to a focalization angle of 27° in air medium). In this case, the paraxial and scalar approximations are still valid. Indeed, Fig. 4, giving the transverse profile of the three field components and the resultant intensity in the focal plane using the former parameters, shows that although the field is not strictly linearly polarized as foreseen before, $E_y \ll E_z \ll E_x$, and we can thus consider that only E_x is different from zero with a good approximation. Note that the exact expression would not intrinsically change the problem, as our scheme can be adapted to any field profile discrimination.

B. Reflection onto the disk

In order to compute the reflected field, we simply assume that bumps and holes are generated in such a way that they induce a π phase shift between them at reflection on the field profile. Note that the holes' depth is usually $\lambda/4$, but precise calculations would be required to give the exact shape of the pits, as they are supposed to be burnt below the wavelength size, and as the field penetration in those holes is not trivial [4–6]. As we have shown that only one vectorial component of the field was relevant in the focal plane, we can directly apply this phase shift to the amplitude profile of this component.

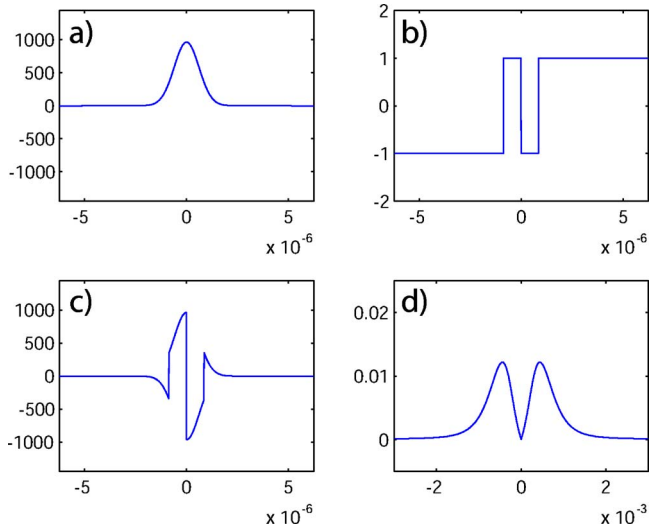

FIG. 5. (Color online) Modifications of the transverse amplitude field profile trough propagation, in the case of a 111 bit sequence in the focal spot: (a) incoming beam profile; (b) 111 bit sequence; (c) corresponding reflected field in the disk plane; (d) far field profile in the detector plane.

We first envision a scheme with only three bits in the focal spot, which means that 2^3 different bit sequences, i.e., a byte, have to be distinguished from each other, using the information extracted from the reflected field. Note that we neglect the influence of other bits in the neighborhood. A more complete calculation involving this effect with more bits will be considered in a further approach.

The amplitude profiles obtained when the incident beam is centered on a bit of the CD are presented on Fig. 5, for a particular bit sequence. Note that we have chosen the space between two bits on the disk equal to the waist size of the reading beam. The first three curves, respectively, show the field amplitude profile incident on the disk, an example of a bit sequence, and the corresponding profile just after reflection onto the disk. We see that binary information is encoded from bumps and holes on the CD to phase flips in the reflected field.

C. Back propagation to the detector plane

In order to extract the information encoded in the transverse amplitude profile of the beam, the field has to be back propagated to the detector plane. A circulator, composed of a polarizing beam splitter and a Faraday rotator, ensures that the linearly polarized reflected beam reaches the array detector, as shown in Fig. 1. Assuming that the detector is positioned just behind the lens plane, the expression of the detected field is given by the far field of the disk plane, apertured by the diameter of the focusing lens. As the focal length and the diameter of the lens are large compared to the wavelength, we use the Rayleigh Sommerfeld integral to compute the field in the lens plane [30]. As an example, the calculated far field profile when the bit sequence 111 is present in the focal spot is shown on the fourth graph of Fig. 5.

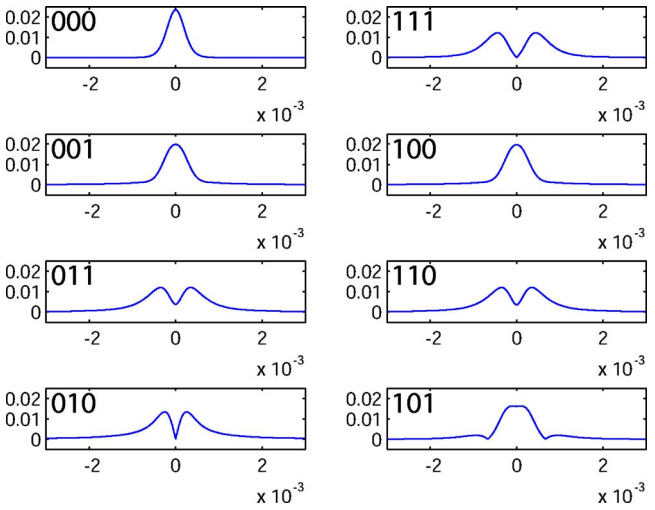

FIG. 6. (Color online) Field profiles in the array detector plane, for each of the 8 bit sequence configuration. Note that they are clearly distinguishable, except for the bit sequences 100 and 001, and 011 and 110, which have the same profile because of the symmetry of the bit sequence relative to the position of the incident laser beam.

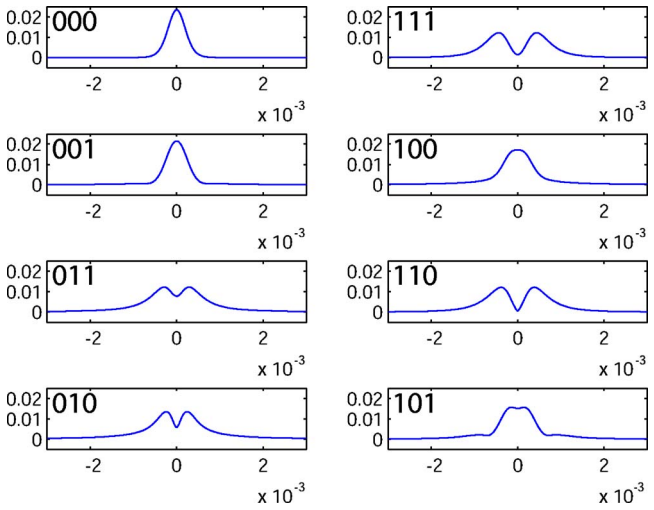

FIG. 7. (Color online) Field profiles in the array detector plane, for each of the 8 bit sequence configuration, when the position of the disk has been shifted of $w_0/6$ relative to the incident beam. The profile degeneracy for 100 and 001, and 011 and 110 is raised. Note that the other profiles have experienced a much smaller shape modification between the two positions of the disk.

The presence of the lens provides a limited aperture for the beam and cuts the high spatial frequencies of the field, which can be a source of information loss, as the difference between each bit sequence can rely on those high frequencies. However, we will see that enough information remains in the low frequency part of the spatial spectrum, so that the 8 bits can be distinguished. This is due to the fact that we have in this problem a lot of *a priori* information on the possible configurations to distinguish.

We see in Fig. 6 that, with the physical parameters used in compact disk readout devices, 6 over 8 profiles in the detector plane are still different enough to be distinguished. At this stage, we are nevertheless unable to discriminate between symmetric configurations, because they give rise to the same far field profile. Therefore, 100 and 001, and 110 and 011, cannot be distinguished. Note that this problem can be solved thanks to the rotation of the disk. Indeed, an asymmetry is created when the position of the disk relative to the laser beam is shifted, thus modifying differently the two previously indistinguishable profiles. As shown in Fig. 7, where the far field profiles are represented after a shift of $w_0/6$ in the position of the disk, the degeneracy has been removed. Moreover, it is important to note that the other profiles experience a small shape modification. This redundant information is very useful in order to remove ambiguities while the disk is rotating.

IV. INFORMATION EXTRACTION FOR BIT SEQUENCE RECOGNITION

In this section, we describe the detection, present some illustrative results, and the way they can be used to increase the readout precision of information encoded on optical disks. We show here that a pixellized detector with a very small number of pixels is enough to distinguish between the 8 bit sequences. Note that for technical and computing time reasons, it is not realistic to use a charge-coupled device (CCD) camera to record the reflected images, as such cameras cannot yet combine good quantum efficiency and high speed.

A. Detected profiles

For simplicity reasons, we limit our calculation to a 5 pixels array detector $D_1,\ldots,D_5$, each of whom has an electronic gain $\sigma_1,\ldots,\sigma_5$, as shown in Fig. 8 The size of each detector has been chosen without a systematic optimi-

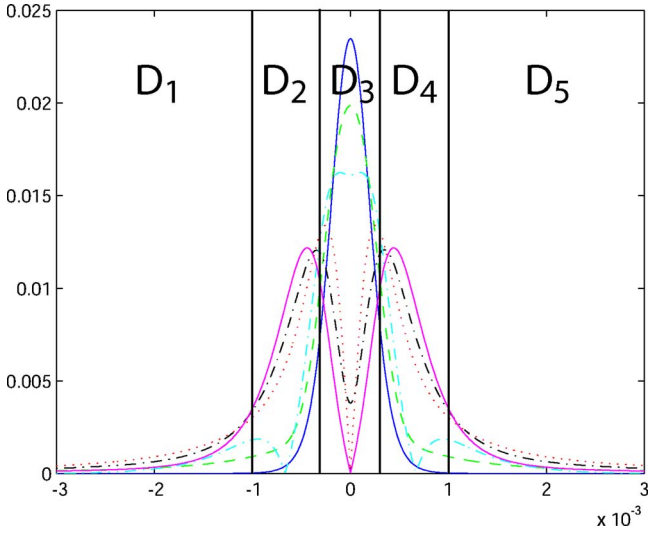

FIG. 8. (Color online) Far field profiles for each bit configuration, and array detector geometry. The 5 detectors $D_1,\ldots,D_5$ have electronic gains $\sigma_1(i),\ldots,\sigma_5,\ldots,(i)$ according to the bit sequence i which is present in the focal spot.

zation, which will be done in a further approach. Gain values are adapted to detect a mean signal equal to zero for each bit configuration present in the focal spot, in order to cancel the common mode classical noise present in the mean field [10]. It means that for each bit sequence i, gains are chosen to satisfy the following relation:

$$\sum_{k=1}^{5} \sigma_k(i) N_k(i) = 0, \tag{2}$$

where $N_k(i)$ is the mean photon number detected on pixel D_k when bit i is present in the focal spot on the disk

$$N_k(i) = \int_{D_k} n_i(x) dx, \tag{3}$$

where $n_i(x)$ is the number of photons incident on the array detector, at position x, when the bit sequence i is present in the focal spot.

As all profiles are symmetrical when the incident beam is centered on a bit, we have set $\sigma_1 = \sigma_5$ and $\sigma_2 = \sigma_4$. In addition, we have chosen $\sigma_3 = -\sigma_1/2$. Using these relations and Eq. (2), we compute gain values adapted to the recognition of each bit sequence. Note that the calculation of each gain configuration requires *a priori* information on the far field profiles, or at least an experimental calibration using a well-known sample.

Now that these gain configurations are set, we can investigate for a bit sequence on the optical disk.

B. Classical results

The expression of the detected signal $S_i(j)$ is given by

$$S_i(j) = \sum_{k=1}^{5} \sigma_k(j) N_k(i), \tag{4}$$

where i refers to the bit sequence effectively present in the focal spot, and j to the gain set adapted to the detection of the bit sequence j. It merely corresponds to the intensity weighted by the electronic gains. Note that for $i=j$—and only in this case if the detector is well chosen—the mean value of the signal $S_i(i)$ is equal to zero, according to Eq. (2). All possible values of $S_i(j)$ are presented for a total number of incident photons $N_{inc}=25$, in Table I where i is read vertically, and corresponds to the bit sequence on the disk, whereas j is read horizontally and refers to the gain set adapted to the detection of bit j. In order not to have redundant information, we have gathered results corresponding to identical far field profiles. A zero value is obtained for only one gain configuration, allowing an identification of the bit sequence present in the focal spot.

The reading process to determine which bit sequence is lit on the disk follows these few steps: the time dependent intensity is first measured on each of the five detectors with all electronic gains set to 1; these intensities are integrated for a time T; the signal is then calculated, using the different gain configurations j; the bit sequence effectively present in the focal spot is determined by the only signal yielding a zero value. Note that the second step just corresponds to the N_k measurements. The integration time T is chosen as the time interval during which the signal leads to the determination of a unique bit sequence. The third step corresponds to the simple calculation of a line in Table I. This can be done in parallel thanks to the speed of data processing on dedicated processors, and the reading rate will thus not be affected compared to current devices. Finally, note that the last step requires a good choice of the parameters in order to be able to distinguish all bit sequences. It means that the noise level has to be smaller than the difference between the two closest values from 0, in order to get a zero mean value for only one bit sequence. Indeed, there must be no overlap between the expectation values when we take into account the noise and thus the uncertainty relative to each measurement. Note that using the zero value as the discriminating factor could be combined with the use of all the calculated values, as each line of Table I is distinct. We just need to know how to weight each data point according to the noise related to its obtention.

TABLE I. Detected signals $S_i(j)$ where i is read vertically and corresponds to the bit sequence on the disk, whereas j is read horizontally and refers to the gain set adapted to the detection of bit j. A zero value means that the tested gain configuration is adapted to the bit sequence.

	000	001/100	010	011/110	101	111
000	0	−34	−204	−254	−77	−303
001/100	15	0	−76	−99	−19	−121
010	23	20	0	−6	16	−13
011/110	24	22	5	0	19	−5
101	19	11	−36	−50	0	−63
111	24	23	9	5	20	0

V. NOISE CALCULATION

A. The shot noise limit

To include the noise in our calculation, we separate classical and quantum noise contributions. The classical noise comprises residual noise of the laser diode, mechanical, and thermal vibrations. The major part of this noise is directly proportional to the signal, i.e., to the number of detected photons. For a detection of the total number of photons N_{inc} in the whole beam during the integration time of the detector, the classical noise contribution $\sqrt{\langle \delta N_{inc}^2 \rangle}$ would thus be written as

$$\sqrt{\langle \delta N_{inc}^2 \rangle} = \beta N_{inc}, \tag{5}$$

where β is a constant factor. And the individual noise variable $\delta N_i(k)$ arising from detection on pixel D_k is given by

$$\delta N_i(k) = \frac{N_i(k)}{N_{inc}} \delta N_{inc}. \tag{6}$$

Using Eqs. (4)–(6) a simple calculation yields the variance of the signal arising from the classical noise

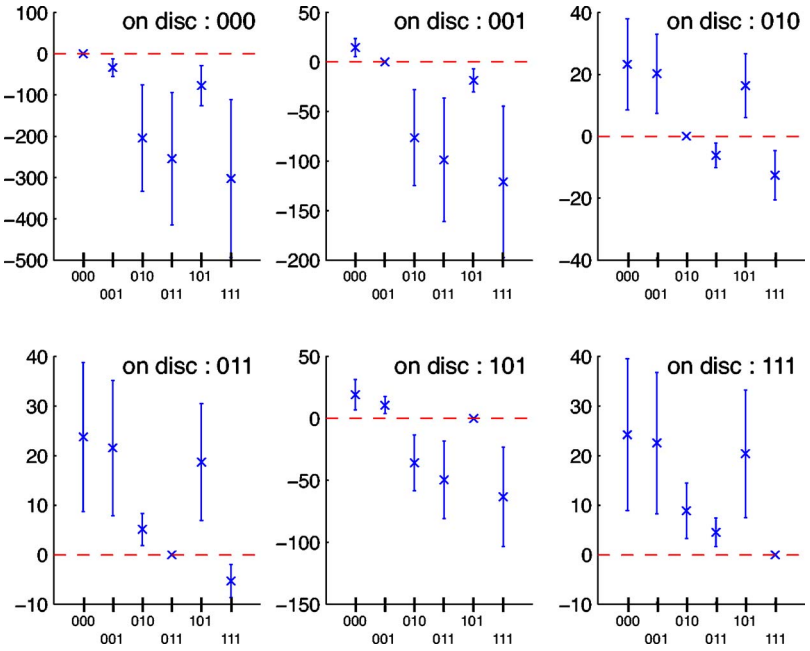

FIG. 9. (Color online) Classical noise (10 dB of excess noise) represented as error bars, for $\lambda = 0.78\ \mu$m, NA=0.47, and 25 detected photons. Each inset corresponds to the 6 signals obtained for the different gain configurations, when one particular bit sequence is present in the focal spot. Each bit sequence present in the focal spot can be clearly identified as only one gain configuration can give a zero value for each inset.

$$\langle \delta \hat{S}_i^2(j) \rangle_{Cl} = \frac{BS_i^2(j)}{N_{inc}}, \tag{7}$$

where the constant $B = N_{inc}\beta^2$ is the classical noise factor, and is chosen so that, when $B=1$ and when all the intensity is detected by one detector, the classical noise term is equal to the shot noise term. Note that classical noise does not deteriorate measurements having a zero mean value. For this reason, we have chosen to discriminate bit sequences by choosing gains such as $S_i(i)=0$, as mentioned earlier.

The calculation of the quantum contribution requires the use of quantum field operators, describing the quantum fluctuations in all transverse modes of the field. By changing the gain configuration of the array detector, not only the signal $S_i(j)$ is modified, but also the related quantum noise denoted $\langle \delta \hat{S}_i^2(j) \rangle_{Qu}$, as different gain configurations are sensitive to noise in different modes of the field. We have shown in Ref. [10] that for a multipixel detection of an optical image, the measurement noise arises from only one mode component of the field, referred to as the *detection mode*, or *noise mode* [31,32]. The expression of the quantum noise is then

$$\langle \delta \hat{S}_i^2(j) \rangle_{Qu} = f_{i,j}^2 N_{inc} \langle \delta \hat{X}_{w_{i,j}}^2 \rangle, \tag{8}$$

where $\delta \hat{X}_{w_{i,j}}$ is the quantum noise contribution of the noise-mode $w_{i,j}(x)$ which is defined for one set of gain j, when the bit sequence i is present in the focal spot, as

$$w_{i,j}(x) = \frac{\sigma_k(j) n_i(x)}{f_{i,j}}, \quad \forall\, x \in D_k \tag{9}$$

and where $f_{i,j}$ is a normalization factor, which expression is

$$f_{i,j}^2 = \frac{\sum_{k=1}^{5} \sigma_k^2(j) N_k(i) dx}{N_{inc}}. \tag{10}$$

The noise mode corresponds in fact to the incident field profile weighted by the gains. The shot noise level corresponds to $\langle \delta \hat{X}_{w_{i,j}}^2 \rangle = 1$.

The variance of the signal can eventually be written as

$$\langle \delta \hat{S}_i^2(j) \rangle = f_{i,j}^2 N_{inc} \langle \delta \hat{X}_{w_{i,j}}^2 \rangle + \frac{BS_i^2(j)}{N_{inc}}. \tag{11}$$

We have first represented the classical noise with an excess noise of 10 dB, as error bars for each result $S_i(j)$, in Fig. 9. We have chosen a representation with a number of detected photons of only 25. Each of the six insets refers to the measurement obtained for a particular bit sequence in the focal spot. The six data points and associated error bars refer to the results obtained when the six gain configurations are tested. One inset thus corresponds to one line in Table I. We can see that with this choice of parameters, the bit sequence effectively present in the focal spot can be determined without ambiguity by the only zero value. The sequence corresponds to the one for which the gains were optimized. We see that the bit sequence discrimination can be achieved even with a very low number of photons. The relative immunity to classical noise of our scheme arises from the fact that measurements are performed around a zero mean value. Thus, given this limit in the minimum necessary photon number and the flux of photons one can calculate the maximum data rate, which is found to be 2×10^7 Mbits/s (this estimation takes into account an integration time T corresponding to $\frac{1}{10}$ of the delay between the readout process of two adjacent bits with a 1 mW laser). This very high value shows that classical noise should not be a limit for data rates in such a scheme.

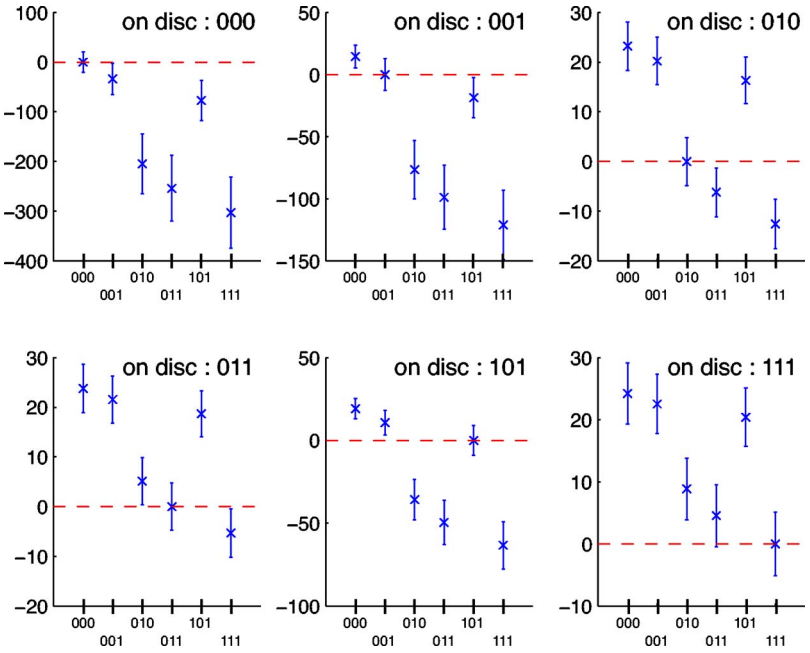

FIG. 10. (Color online) Shot noise represented as error bars, for $\lambda=0.78\ \mu$m, NA $=0.47$, 25 detected photons. Some bit sequences cannot be determined without ambiguity because of the noise level.

The effect of quantum noise is very small, but becomes a limiting factor for such a small number of detected photons, or for a large number of bits encoded on the disk in the wavelength size. In order to see independently the effect of each contribution to the noise, we have thus represented in Fig. 10 the shot noise also for 25 detected photons, appearing as the threshold under which it is impossible to distinguish bit sequences because of the quantum noise. Note that for the represented case, the shot noise is the most important contribution, and that it prevents a bit sequence discrimination, as a zero value for the signal can be obtained for several gain configurations in the same inset.

B. Beyond the shot noise limit

When the shot noise is the limiting factor, nonclassical light can be used to perform measurements beyond the quantum noise limit. We have shown in Ref. [10] that squeezing the noise mode of the incident field was a necessary and sufficient condition to a perfect measurement. What we are interested in is improving the measurements that yield a zero value, which are obtained when the gain configuration matches the bit sequence in the focal spot, as $S_i(i)=0$. Using Eq. (11), we see that $w_{i,i}$ has to be squeezed. As no information on the bit present in the focal spot is available before the measurement, in order to improve simultaneously all the bit sequence detections, the six noise modes have to be squeezed at the same time in the incident field. These six transverse modes are not necessarily orthogonal, but one can show that squeezing the subspace that can generate all of them is enough to induce the same amount of squeezing.

The quantum noise with 10 dB of squeezing on the subspace generated by the $w_{i,i}$ is represented as error bars in Fig.

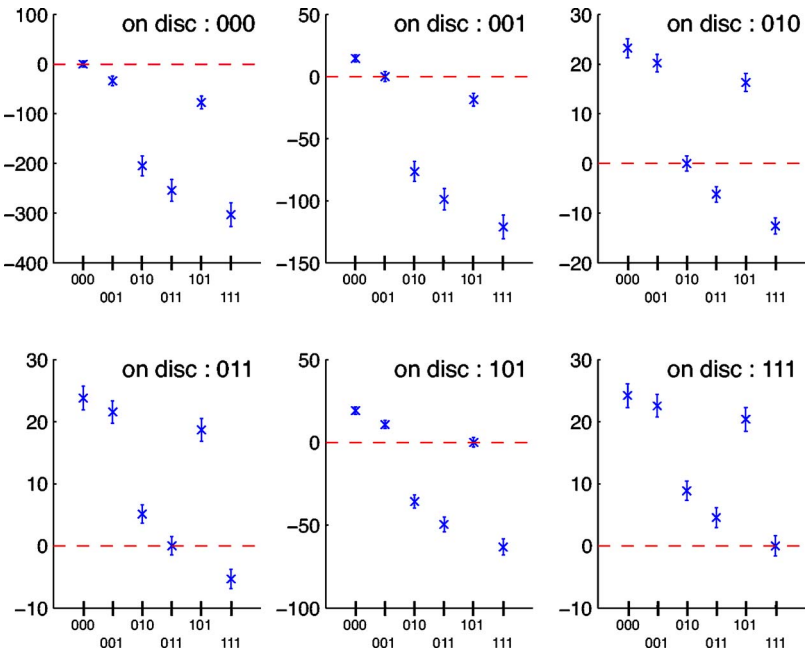

FIG. 11. (Color online) Quantum detection noise represented as error bars, for $\lambda=0.78\ \mu$m, NA$=0.47$, 25 detected photons and -10 dB of simultaneous squeezing for all the flipped modes. The ambiguity in the presence of shot noise has been removed and each bit sequence can be identified.

11. The noise of each noise-mode $w_{i,j}$ is computed using its overlap integrals with the generator modes of the squeezed subspace, assuming that all modes orthogonal to the squeezed subspace are filled with coherent noise. In this case, the effect of squeezing, reducing the quantum noise on the measurements, and especially on the measurement for which the gains have been optimized, is enough to discriminate bit sequences that were masked by quantum noise.

VI. CONCLUSION

We have proposed a way of information extraction from optical disks, based on a multipixel detection. We have first demonstrated, using only classical resources, that this detection could allow large data storage capacity, by burning several bits in the spot size of the reading laser. We have presented a proof of principle through a simple example which will be refined in further studies. We have also shown that in shot noise limited measurements, using squeezed light in appropriate modes of the incident laser beam can lead to improvement in bit sequence discrimination.

The next steps are to study in detail how to extract the redundant information when the disk is spinning, and to systematically optimize the number of bits in the focal spot, the number and size of pixels in the array detector. Such a regime involving a large number of bits in the focal spot will ultimately be limited by the shot noise, and will require the quantum noise calculations presented in this paper.

ACKNOWLEDGMENTS

We thank Magnus Hsu, Ping Koy Lam and Hans Bachor for fruitful discussions. Laboratoire Kastler Brossel, of the Ecole Normale Superieure and University Pierre et Marie Curie, is associated to CNRS. This work has been supported by the European Union in the frame of the QUANTIM network (Contract No. IST 2000-26019).

[1] H. A. Bethe, Phys. Rev. **7**, 66 (1944); **8**, 163 (1944).
[2] D. S. Marx and P. Psaltis, J. Opt. Soc. Am. A **14**, 1268 (1997).
[3] D. S. Marx and P. Psaltis, Appl. Opt. **36**, 6434 (1997).
[4] X. Wang, J. Mason, M. Latta, T. C. Strand, D. S. Marx, and P. Psaltis, J. Opt. Soc. Am. A **18**, 565 (2001).
[5] W.-C. Liu and M. W. Kowarz, Appl. Opt. **38**, 3787 (1999).
[6] J. M. Brok and H. P. Urbach, J. Opt. Soc. Am. A **20**, 256 (2003).
[7] I. Sokolov and M. Kolobov, Opt. Lett. **29**, 703 (2004).
[8] M. T. L. Hsu, W. P. Bowen, V. Delaubert, C. Fabre, H.-A. Bachor, and P. K. Lam (unpublished).
[9] P. Török (unpublished).
[10] N. Treps, V. Delaubert, A. Maître, J. M. Courty, and C. Fabre, Phys. Rev. A **71**, 013820 (2005).
[11] A. G. van Nie, Philips Res. Rep. **19**, 378 (1964); **19**, 394 (1964).
[12] M. Lax, W. H. Louisell, and W. B. McKnight, Phys. Rev. A **11**, 1365 (1975).
[13] S. R. Seshadri, J. Opt. Soc. Am. A **19**, 2134 (2002), and references therein.
[14] A. Ciattoni, B. Crosignani, and P. Di Porto, Opt. Commun. **177**, 9 (2000).
[15] Q. Cao and X. Deng, J. Opt. Soc. Am. A **15**, 1144 (1998).
[16] B. T. Landesman and H. H. Barrett, J. Opt. Soc. Am. A **5**, 1610 (1988).
[17] G. Rodriguez-Morales and S. Chavez-Cerda, Opt. Lett. **5**, 430 (2004).
[18] Z. Ulanowski and I. K. Ludlow, Opt. Lett. **25**, 1792 (2000).
[19] T. A. Nieminen, H. Rubinsztein-Dunlop, and N. R. Heckenberg (unpublished).
[20] B. Richards and E. Wolf, Proc. R. Soc. London, Ser. A **253**, 359 (1959).
[21] S. Quabis, R. Dorn, M. Eberler, O. Glöckl, and G. Leuchs, Appl. Phys. B **72**, 109 (2001).
[22] L. Novotny, R. D. Grober, and K. Karrai, Opt. Lett. **26**, 789 (2001).
[23] R. Dorn, S. Quabis, and G. Leuchs, Phys. Rev. Lett. **91**, 233901 (2003).
[24] S. Quabis, R. Dorn, M. Eberler, O. Glöckl, and G. Leuchs, Opt. Commun. **179**, 1 (2000).
[25] C. J. R. Sheppard, J. Opt. Soc. Am. A **18**, 1579 (2001).
[26] P. Török, P. Varga, Z. Laczik, and G. R. Booker, J. Opt. Soc. Am. A **12**, 325 (1995).
[27] K. S. Youngworth and T. G. Brown, Opt. Express **7**, 77 (2000).
[28] Q. Zhan and J. R. Leger, Opt. Express **10**, 324 (2002).
[29] A. E. Siegman, *Lasers* (University Science, Mill Valley, CA, 1986).
[30] M. Born and E. Wolf, *Principle of Optics* (Cambridge University Press, 1959).
[31] V. Delaubert, N. Treps, C. C. Harb, P. K. Lam, and H.-A. Bachor e-print arxiv/ quant-ph/0512151
[32] N. Treps, N. Grosse, W. P. Bowen, M. T. L. Hsu, A. Maître, C. Fabre, H.-A. Bachor, and P. K. Lam, J. Opt. B: Quantum Semiclassical Opt. **6**, S664 (2004).